iScience

CellPress
OPEN ACCESS

Article

Ventral zona incerta parvalbumin neurons modulate sensory-induced and stress-induced self-grooming via input-dependent mechanisms in mice

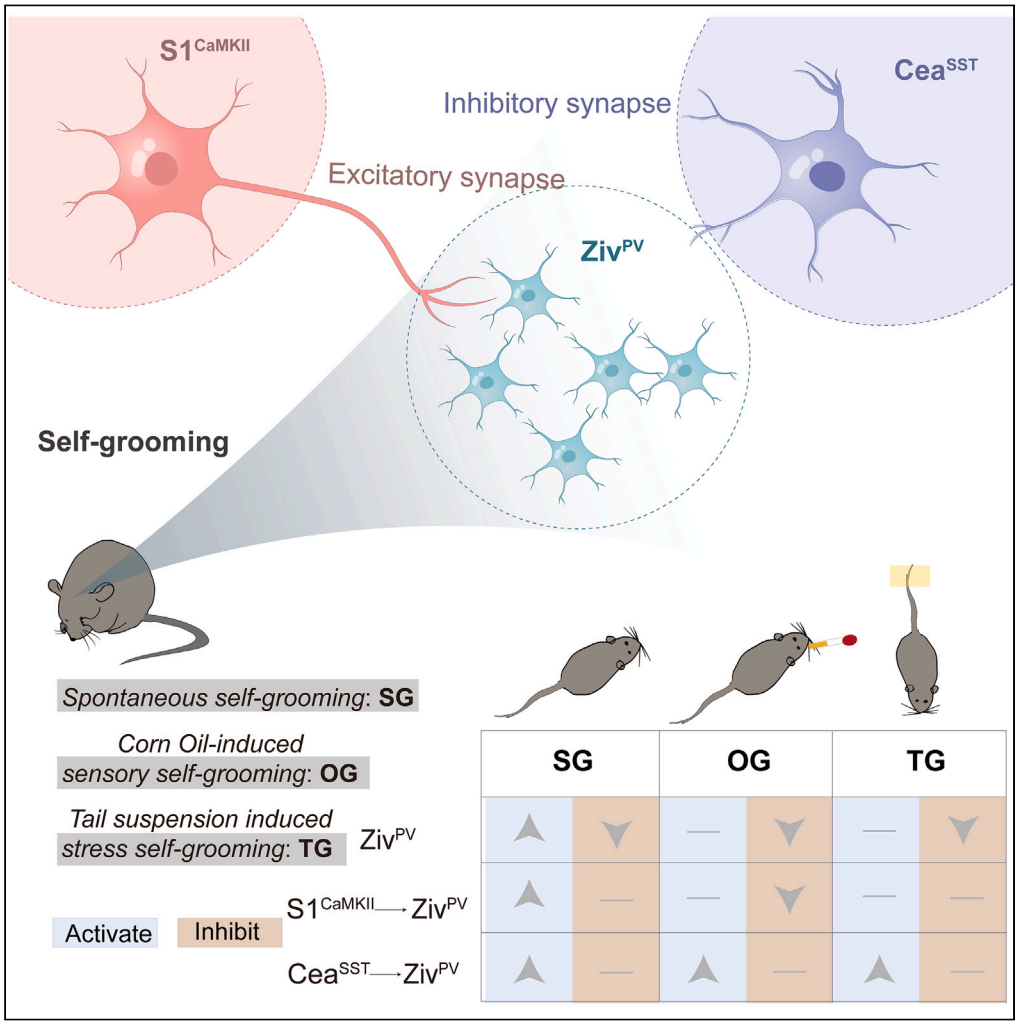

Junye Ge, Pengfei Ren, Biqing Tian, ..., Shengxi Wu, Qian Xue, Wenting Wang

xueqianj@fmmu.edu.cn (Q.X.)
wwt0657@fmmu.edu.cn (W.W.)

Highlights

Ventral zona incerta (Ziv) involved in self-grooming

Ziv regulates sensory-induced and stress-induced self-grooming

Sensory and emotional information was processed by inputs from S1 and CeA to Ziv

Ge et al., iScience 27, 110165
July 19, 2024
https://doi.org/10.1016/j.isci.2024.110165

iScience

CellPress
OPEN ACCESS

Article

Ventral zona incerta parvalbumin neurons modulate sensory-induced and stress-induced self-grooming via input-dependent mechanisms in mice

Junye Ge,[1,2,4] Pengfei Ren,[2,4] Biqing Tian,[2,4] Jiaqi Li,[3] Chuchu Qi,[2] Qiyi Huang,[2] Keke Ren,[2] Erling Hu,[2] Honghui Mao,[2] Ying Zang,[1] Shengxi Wu,[2] Qian Xue,[2,*] and Wenting Wang[2,5,*]

SUMMARY

Self-grooming is an innate stereotyped behavior influenced by sense and emotion. It is considered an important characteristic in various disease models. However, the neural circuit mechanism underlying sensory-induced and emotion-driven self-grooming remains unclear. We found that the ventral zona incerta (Ziv) was activated during spontaneous self-grooming (SG), corn oil-induced sensory self-grooming (OG), and tail suspension-induced stress self-grooming (TG). Optogenetic excitation of Ziv parvalbumin (PV) neurons increased the duration of SG. Conversely, optogenetic inhibition of Ziv^{PV} neurons significantly reduced self-grooming in all three models. Furthermore, glutamatergic inputs from the primary sensory cortex activated the Ziv and contributed to OG. Activation of GABAergic inputs from the central amygdala to the Ziv increased SG, OG, and TG, potentially through local negative regulation of the Ziv. These findings suggest that the Ziv may play a crucial role in processing sensory and emotional information related to self-grooming, making it a potential target for regulating stereotyped behavior.

INTRODUCTION

Self-grooming is a complex innate behavior that is commonly observed in rodents.[1,2] This behavior has a well-preserved sequence pattern and serves various important physiological functions, such as hygiene maintenance, thermoregulation, social communication, de-arousal, and stress regulation.[1–3] Moreover, under pathological conditions, these normal self-grooming functions can be disrupted. Abnormal self-grooming behavior has been observed in animal models of different diseases, including obsessive-compulsive disorder,[4,5] autism,[6–9] and anxiety disorder.[10,11]

Clean fur and self-soothing are two primary functions of self-grooming in rodents. By engaging in self-grooming, rodents can maintain hygiene and reduce the risk of acquiring diseases.[1] This behavior can be triggered by increased sensory input, such as the application of corn oil[12] or capsaicin to the orofacial area of mice,[12,13] or by exposing mice to water squirts.[14,15] These instances of self-grooming are referred to as sensory self-grooming. Additionally, rodents may exhibit increased self-grooming behaviors in response to stress.[1,7,11,12,15,16] For example, mice may engage in extensive grooming after being restrained in a tube[15] or experiencing an electric shock.[12,17] This behavior may serve as an adaptive response to stress or a restraining force to prevent overresponse to stress and is classified as stress self-grooming.[1,17–19]

Previous studies have provided a framework for studying the neural circuits involved in self-grooming. The corticostriatal circuit,[18,20–23] cerebellum,[24,25] and spinal trigeminal nucleus[12] have been reported to play a role in the locomotion and rhythm of self-grooming. Additionally, the amygdala and hypothalamus may be involved in the emotional aspects of self-grooming, and the sensory cortex is responsible for the sensory information during self-grooming.[15,26–29] However, a region may be needed to converge the different information, including the sensory and emotional information, to regulate self-grooming. The zona incerta (ZI), a region between the dorsal thalamus and subthalamic nucleus, has been identified as an integrative node of circuits for global behavioral modulation.[30] It has extensive connectivity with other brain regions and is involved in innate instinctive behaviors, including binge eating,[31] sleeping,[32] predatory hunting,[33,34] defensive behavior,[35] and investigatory and seeking behavior.[36,37] Recent studies have also shown that the ZI is involved in pain[38–40] and itching,[41] which are closely related to the behavior pattern of self-grooming. However, the specific identity and neural mechanisms of the ZI related to self-grooming remain unknown.

[1]Pain Research Center and Department of Physiology, Zhongshan Medical School, Sun Yat-sen University, 74 Zhongshan Road. 2, Guangzhou 510080, China
[2]Department of Neurobiology, School of Basic Medicine, Fourth Military Medical University, Xi'an, Shaanxi 710032, China
[3]School of Life Science and Technology, ShanghaiTech University, Shanghai 201210, China
[4]These authors contributed equally
[5]Lead contact
*Correspondence: xueqianj@fmmu.edu.cn (Q.X.), wwt0657@fmmu.edu.cn (W.W.)
https://doi.org/10.1016/j.isci.2024.110165

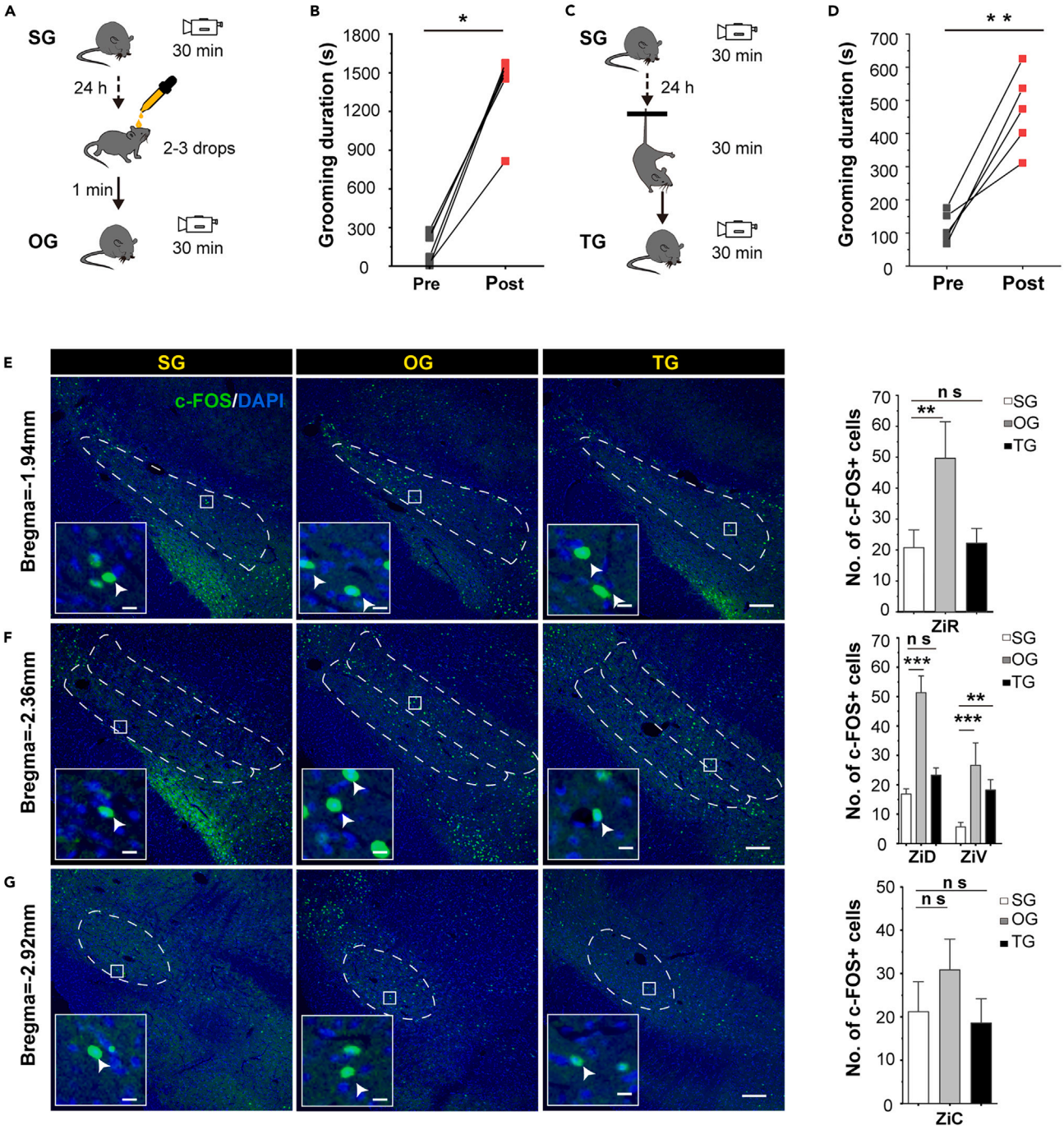

Figure 1. The involvement of Ziv in OG and TG

(A) Schematics of the corn oil-induced sensory self-grooming (OG) behavioral experiment design.

(B) The total self-grooming duration before and after dripping corn oil. *Wilcoxon signed-rank test* ($n = 6$): $Z = -2.201$, $p = 0.028$. *$p < 0.05$.

(C) Schematics of the tail suspension-induced stress self-grooming (TG) behavioral experiment design.

(D) The total self-grooming duration before and after tail suspension. Two-tailed paired t test ($n = 5$): $t = -6.244$, $df = 4$, $p = 0.003$. **$p < 0.01$.

(E) Left, representative images of three groups (Control, OG, and TG) showing c-Fos protein (green) and site of magnified inset box indicated in the rostral sector of the ZI (Zir). Scale bars for image and inset are 100 μm and 10 μm, respectively. Right, quantification of c-Fos+ cells number of three groups (Control, OG, and TG) in Zir. *One-factor ANOVA* and *Bonferroni correction* for *post hoc* test ($n = 8$ in the control group, $n = 6$ in the OG group and 10 in the TG group): $F(2,21) = 10.444$, $p = 0.001$; $p_{control\&OG} = 0.002$, $p_{control\&TG} = 1$. **$p < 0.01$. Data are represented as mean ± SEM.

Figure 1. *Continued*

(F) Left, representative images of three groups (Control, OG, and TG) showing c-Fos protein (green) and site of magnified inset box indicated in the dorsal sector of the ZI (Zid) and Ziv. Scale bars for image and inset are 100 μm and 10 μm, respectively. Right, quantification of c-Fos+ cells number of three groups (Control, OG, and TG) in Zir and Ziv. For the Zid, *Kruskal-Wallis H test* followed by *Nemenyi multiple comparisons test* ($n = 9$ in the control group, $n = 11$ in the OG group and 9 in the TG group): $\chi^2 = 23.395$, $df = 2$, $p = 0$; $\chi^2_{control\&OG} = 22.72$, $p_{control\&OG} = 0$; $\chi^2_{control\&TG} = 3.44$, $p_{control\&TG} = 0.18$. $^{**}p < 0.01$. For the Ziv, *Kruskal-Wallis H test* followed by *Nemenyi multiple comparisons test*: ($n = 9$ in the control group, $n = 11$ in the OG group and 9 in the TG group): $\chi^2 = 18.108$, $df = 2$, $p = 0$; $\chi^2_{control\&OG} = 17.06$, $p_{control\&OG} = 0$; $\chi^2_{control\&TG} = 9.3$, $p_{control\&TG} = 0.01$. $^{**}p < 0.01$, $^{***}p < 0.001$.

(G) Left, representative images of three groups (Control, OG, and TG) showing c-Fos protein (green) and site of magnified inset box indicated in the caudal sector of the ZI (Zic). Scale bars for image and inset are 100 μm and 10 μm, respectively. Right, quantification of c-Fos+ cells number of three groups (Control, OG, and TG) in Zic. *One-factor ANOVA* and *Bonferroni correction* for post hoc test ($n = 5$ in the control group, $n = 6$ in the OG group and 5 in the TG group): $F(2,13) = 2.199$, $p = 0.15$; $p_{control\&OG} = 0.438$, $p_{control\&TG} = 1$.

In this study, we used cell type-specific fiber photometry, virus-mediated input-output tracing, electrophysiology, and optogenetics to reveal that the ventral zona incerta (Ziv) is involved in self-grooming and serves as an integrative node of the circuits for sensory-induced self-grooming and stress-induced self-grooming. Glutamatergic inputs from the primary sensory cortex (S1) activate the Ziv and selectively contribute to sensory-induced self-grooming, and GABAergic inputs from the central amygdala (CeA) inhibit the Ziv and participate in both sensory-induced self-grooming and stress-induced self-grooming, which may reveal the complex role of the Ziv in the interaction of feelings and emotions in stereotyped self-grooming behavior.

RESULTS

The Ziv is involved in corn oil-induced sensory self-grooming (OG) and tail suspension-induced stress self-grooming (TG)

We used corn oil as a sensory stimulus and tail suspension[12] as a stress stimulus to induce extensive self-grooming behavior. The self-grooming behavior of the two groups of mice was recorded through video observation for 30 min before and after the application of external stimuli (Figures 1A and 1C). Our results revealed a significant difference in the duration of self-grooming between the pre- and posttest periods for both external stimuli (Figures 1B and 1D).

To investigate the involvement of specific brain regions in both OG and TG, the animals were randomly assigned to three groups: a spontaneous self-grooming (SG) group that was placed alone in the test chamber for 30 min, an OG group that received 100 μL of corn oil on its orofacial region and was then placed in the test chamber for 30 min, and a TG group that was subjected to tail suspension for 20 min followed by placement in the test chamber for 30 min. After 30 min of video recording, all mice were returned to their home cages and perfused 1 h later for staining of the immediate-early gene cellular oncogene (c-FOS) (Figure S1A). In one of our recent studies,[41] we observed that activation of the ZI may be associated with self-grooming. Therefore, the expression of c-FOS in the Ziv was detected first. Interestingly, both the OG and TG groups displayed a significant increase in c-Fos-expressing neurons in the ventral sector of the ZI (Figure 1F). However, the OG group showed a significant increase in the number of c-Fos-expressing neurons in the rostral sector of the ZI, whereas no such difference was observed in the TG group (Figure 1E). Additionally, there were no significant changes in the number of c-Fos-expressing neurons in the caudal sector of the ZI in either the OG group or TG group (Figure 1G). Increased expression of c-FOS was also detected in various regions, such as the anterior cingulate cortex (ACC), basolateral amygdala (BLA), and striatum (Figures S1B and S1C). However, our previous work suggested that the ACC may not be involved in self-grooming.[7] The striatum is known to be involved in modulating self-grooming.[20] Consequently, our subsequent investigation shifted its focus to the Ziv.

Neural activity of Ziv^{PV} neurons during SG, OG, and TG

Previous research has indicated that parvalbumin (PV) neurons constitute the majority of the Ziv.[42] Our results confirmed this finding (Figures S2A–S2D). Therefore, we injected a Cre-dependent adeno-associated virus (AAV) expressing GCaMP6s into the Ziv of PV-internal ribosome entry site (IRES)-Cre mice to determine the activity patterns of Ziv^{PV} neurons during self-grooming behavior (Figures 2A, 2B, S2E, and S2F). By aligning the calcium signals with video recordings of self-grooming behavior, we observed a significant increase in neuronal activity during SG, OG, and TG in awake mice (Figures 2C–2E). We also observed a significant decrease in neuronal activity at the end of self-grooming (Figures S2I and S2J). Changes in calcium signals induced by movement were excluded (Figures S2K and S2L). To quantitatively assess the extent of the calcium signal elevation throughout the self-grooming process, we established a baseline period (−2 to 0 s relative to the onset of self-grooming) and measured the changes in calcium signals within 3 s after self-grooming using the area under the curve (AUC) as an indicator. Our findings revealed a significant increase in single-fluorophore genetically encoded calcium indicators (GCaMP6s) fluorescence in Ziv^{PV} neurons in all the self-grooming models compared to that in the control group (Figures 2C–2E and S2G). Furthermore, this increase was sustained during SG, OG, and TG (Figure S2H). But there is no significant correlation between the AUC and duration of self-grooming (Figure S2M). These results suggested that the Ziv plays a crucial role in self-grooming behavior, as mentioned earlier, and that the Ziv may serve as a potential key modulator influencing self-grooming behaviors triggered by various stimuli.

Ziv^{PV} neurons regulate complicated and diverse self-grooming behavior

To establish a causal relationship between the activities of Ziv^{PV} neurons and self-grooming behavior, optogenetic techniques were employed to selectively activate PV neurons in a Cre-dependent manner (Figure 3A). The functionality and expression of channelrhodopsin-2 (ChR2) in

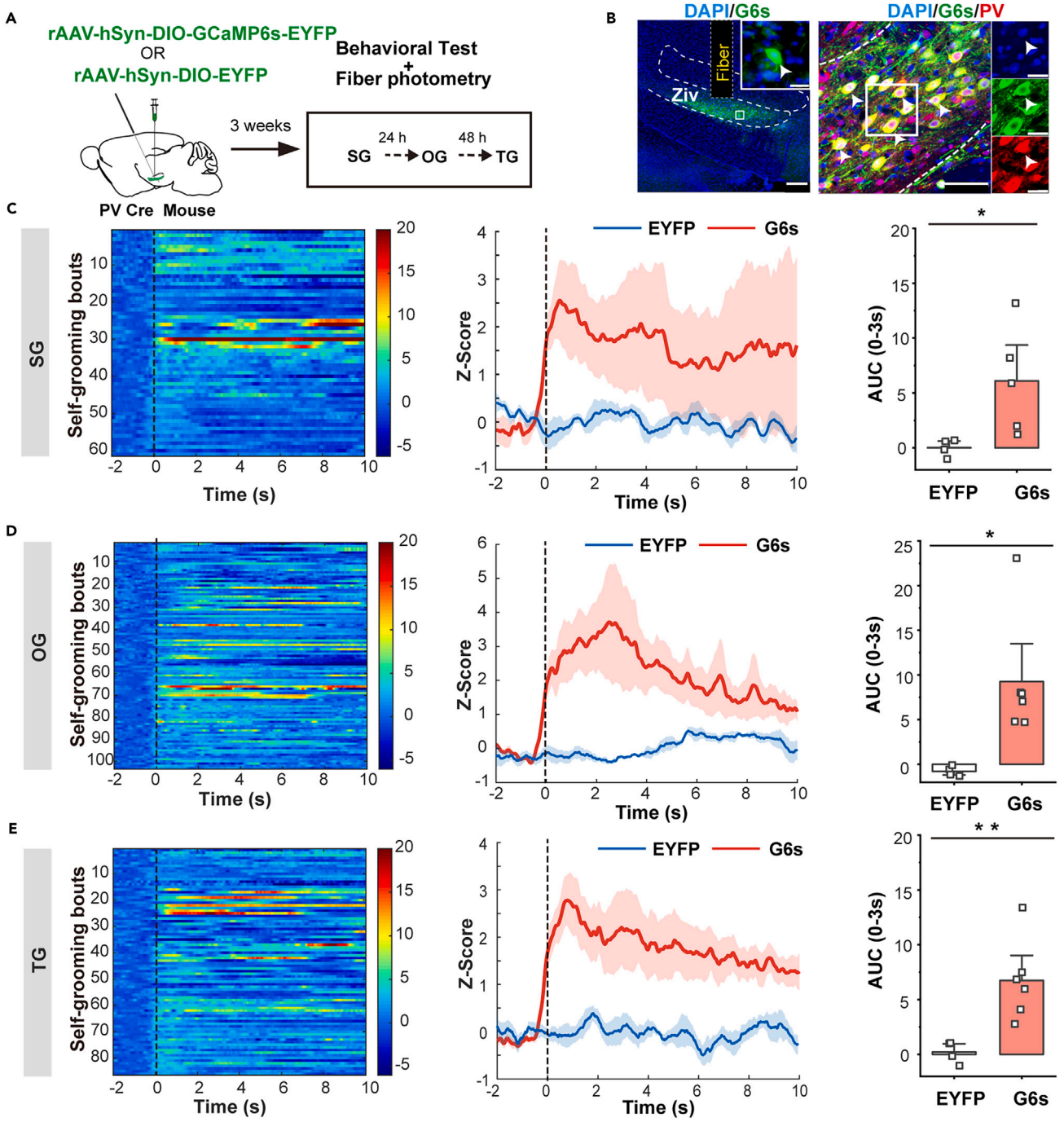

Figure 2. Activation of Ziv^{PV} neurons during three self-grooming models

(A) Schematic representation of the setup of fiber photometry to record calcium activity from Ziv PV + neurons infected with rAAV-hSyn-DIO-GCaMP6s or rAAV-hSyn-DIO-EYFP virus.

(B) Expression of GCaMP6s and placement of the fiber optics were verified postmortem. Scale bar 250 μm (Left). Representative images, counterstained with DAPI (blue), showing GCaMP6s (green) colocalizing with PV protein (red). Left, scale bars for image and inset are 200 μm and 20 μm, respectively. Right, 50 μm for the big image and 20 μm for blown-up images.

(C–E) All results of calcium activity (left panel) and the averaged results of calcium activity (red, middle panel) in Ziv PV + neurons around the start of spontaneous self-grooming (C; red, *n* = 61 trials from 5 mice; blue, *n* = 30 trials from 4 mice.), oil-induced self-grooming (D; *n* = 103 trials from 6 mice; blue, *n* = 35 trials from

Figure 2. *Continued*

4 mice.), and tail suspension-induced self-grooming (E; $n = 86$ trials from 6 mice; blue, $n = 27$ trials from 4 mice). The blue traces represent signals from animals which expressed only EYFP but not GCaMP6s. Right, *two-tailed unpaired t test* ($n = 5$ mice in G6s group and $n = 4$ mice in EYFP group): $t = 2.428$, $df = 7$, $p = 0.046$ (C); *Mann-Whitney U test* ($n = 6$ mice in G6s group and $n = 4$ mice in EYFP group): $Z = -2.558$, $p = 0.011$ (D); two-tailed unpaired t test ($n = 6$ mice in G6s group and $n = 4$ mice in EYFP group): $t = 3.397$, $df = 8$, $p = 0.009$ (C). $^*p < 0.05$, $^{**}p < 0.01$. Data are represented as mean ± SEM.

Ziv^{PV} neurons were confirmed through patch clamp and immunofluorescence staining of brain slices (Figures 3B–3E, S3A, and S3B). Upon delivery of blue light to the Ziv region, an increase in SG was observed (Figures 3F and Video S1), and locomotion was not influenced (Figure S3E, left). However, the delivery of light did not affect OG or TG (Figure 3F). Further analysis of the enhancement rate of the self-grooming time after light exposure revealed that only the enhancement rate of spontaneous self-grooming was significantly greater than zero, while the enhancement rates of the other two models were similar to those of the enhanced yellow fluorescent protein (EYFP) group and did not differ from zero (Figure 3G).

To investigate whether the activity of Ziv^{PV} neurons is necessary for self-grooming behaviors, these neurons were optogenetically inhibited by injecting rAAV-hSyn-DIO-eNPHR3.0-EYFP or rAAV-hSyn-DIO-EYFP (as a control) into the Ziv region of PV-IRES-Cre mice (Figure 3H). The expression of microbial halorhodopsin (NPHR) in Ziv^{PV} neurons was confirmed through experiments conducted on brain slices (Figures 3I, 3J, S3C, and S3D). Surprisingly, the delivery of yellow light to the Ziv region resulted in suppressed self-grooming behavior across all self-grooming models (Figure 3K), and this decrease was not attributed to a decrease in locomotion (Figure S3E, right). The inhibition rate of the self-grooming time after light exposure further confirmed that all three types of self-grooming could be suppressed, while the EYFP group did not exhibit this effect (Figures 3L, S3H, and S3I). Analysis of the number of grooming times and the duration of each grooming episode revealed that the inhibition of Ziv^{PV} neurons primarily suppressed self-grooming by reducing the duration of each grooming episode (Figures S3F and S3G). These results suggested that Ziv^{PV} neurons may serve as important nodes of SG, OG, and TG, especially by receiving and integrating sensory and emotional information from upstream inputs.

Ziv^{PV} neurons receive direct synaptic inputs from $S1^{CaMKII}$ neurons and CeA^{SST} neurons

To identify the presynaptic inputs to Ziv^{PV} neurons, we injected Cre-dependent helper viruses (rAAV-EF1α-DIO-EGFP-T2A-TVA and rAAV-EF1α-DIO-oRVG) into the Ziv of PV-IRES-Cre mice (Figure 4A). After 3 weeks, the rabies virus (RV) (RV-ENVA-ΔG-dsRed) was injected into the same site (Figures 4A and 4B). Through this approach, we were able to identify several brain regions that contribute to the inputs received by Ziv^{PV} neurons. Notably, the S1, which plays a crucial role in sensation (Figure 4C), as well as the CeA (Figure 4E), a region associated with negative emotions,[43–45] were among the identified input regions. Additionally, other brain regions, such as the ACC, lateral septal nucleus (LS), retrosplenial cortex (RSC), primary motor cortex (M1), and specific parts of the lateral posterior thalamic nucleus (LPMR, LPLR), were robustly labeled (Figure S4A), consistent with previous studies.[30] In the S1 and CeA, we observed neurons intensely labeled with dsRed, which colocalized with the Calcium-calmodulin (CaM)-dependent protein kinase II (CaMKII) antibody in the S1 and the somatostatin (SST) antibody in the CeA (Figures 4C and 4E), consistent with previous research.[35,46] To further confirm the connections of the $S1^{CaMKII} \rightarrow Ziv^{PV}$ pathway and the $CeA^{SST} \rightarrow Ziv^{PV}$ pathway, we infused rAAV-CaMKIIα-mCherry into the S1 of C57BL/6J mice and rAAV-DIO-EYFP into the CeA of SST-IRES-Cre mice. mCherry+ (CaMKII) cell bodies in the S1 and numerous mCherry+ fibers in the Ziv were detected (Figure 4D), as were EYFP+ (SST) cell bodies in the CeA and numerous EYFP+ fibers in the Ziv (Figure 4F). Furthermore, rAAV-DIO-*retro*-mCherry was injected into the Ziv of SST-IRES-Cre mice or CaMKII-IRES-Cre mice, and we observed mCherry+ cell bodies in the CeA of SST-IRES-Cre mice (Figures S4B and S4C) and in the S1 of CaMKII-IRES-Cre mice (Figures S4D and S4E). We also detected fiber projections from Ziv^{PV} neurons in other brain regions (Figures S4F and S4G) by injecting rAAV-hSyn-DIO-EYFP into the Ziv of PV-IRES-Cre mice.

The $S1^{CaMKII} \rightarrow Ziv^{PV}$ circuit is necessary for sensory-induced self-grooming but not for stress-induced self-grooming

Subsequently, we investigated the functional connections of the $S1^{CaMKII} \rightarrow Ziv^{PV}$ pathway by injecting rAAV-CaMKIIα-hChR2(H134R)-mCherry into the S1 and rAAV-hSyn-DIO-GCaMP6s into the Ziv of PV-IRES-Cre mice (Figure 5A). After three weeks, fibers were inserted into the S1 and Ziv to activate projection neurons in the S1 and record the calcium activity of PV cells in the Ziv, resulting in a significant increase in the number of Ziv^{PV} neurons (Figure 5B). In acute brain slices, whole-cell voltage-clamp recordings were performed on PV neurons in the Ziv to record optogenetically induced postsynaptic currents (Figures 5C and 5D). These recordings were conducted in the presence of tetrodotoxin and 4-aminopyridine to exclude polysynaptic connections. By sequentially applying inhibitors of glutamate receptors (NBQX), we observed that NBQX significantly inhibited synaptic responses (Figure 5D).

To further investigate whether the $S1^{CaMKII} \rightarrow Ziv^{PV}$ circuit is involved in Ziv-regulated self-grooming, we injected rAAV-CaMKIIα-hChR2(H134R)-EYFP into the S1 and implanted an optical fiber onto the Ziv for optogenetic stimulation of the excitatory $S1^{CaMKII} \rightarrow Ziv^{PV}$ pathway terminals (Figures 5E and S5A). Activation of this pathway triggered self-grooming behavior under normal conditions, similar to the stimulation of the Ziv. When blue light was delivered into the excitatory $S1^{CaMKII} \rightarrow Ziv^{PV}$ pathway terminals in the Ziv, there was an increase in spontaneous self-grooming compared to that in control mice (Figure 5F, left panel). However, light delivery did not affect OG or TG (Figure 5F, middle and right panel). Additionally, we injected rAAV-CaMKIIα-eNpHR3.0-mCherry into the S1 and implanted an optical fiber onto the Ziv for optogenetic stimulation of the excitatory $S1^{CaMKII} \rightarrow Ziv^{PV}$ pathway terminals (Figure 5G). Interestingly, inhibition of this pathway specifically targeted sensory-evoked self-grooming behavior. When yellow light was delivered into the excitatory $S1^{CaMKII} \rightarrow Ziv^{PV}$ pathway terminals in the Ziv, there was a decrease in OG (Figure 5H, middle panel). The total grooming time changes are mostly explained by the average time of each bout

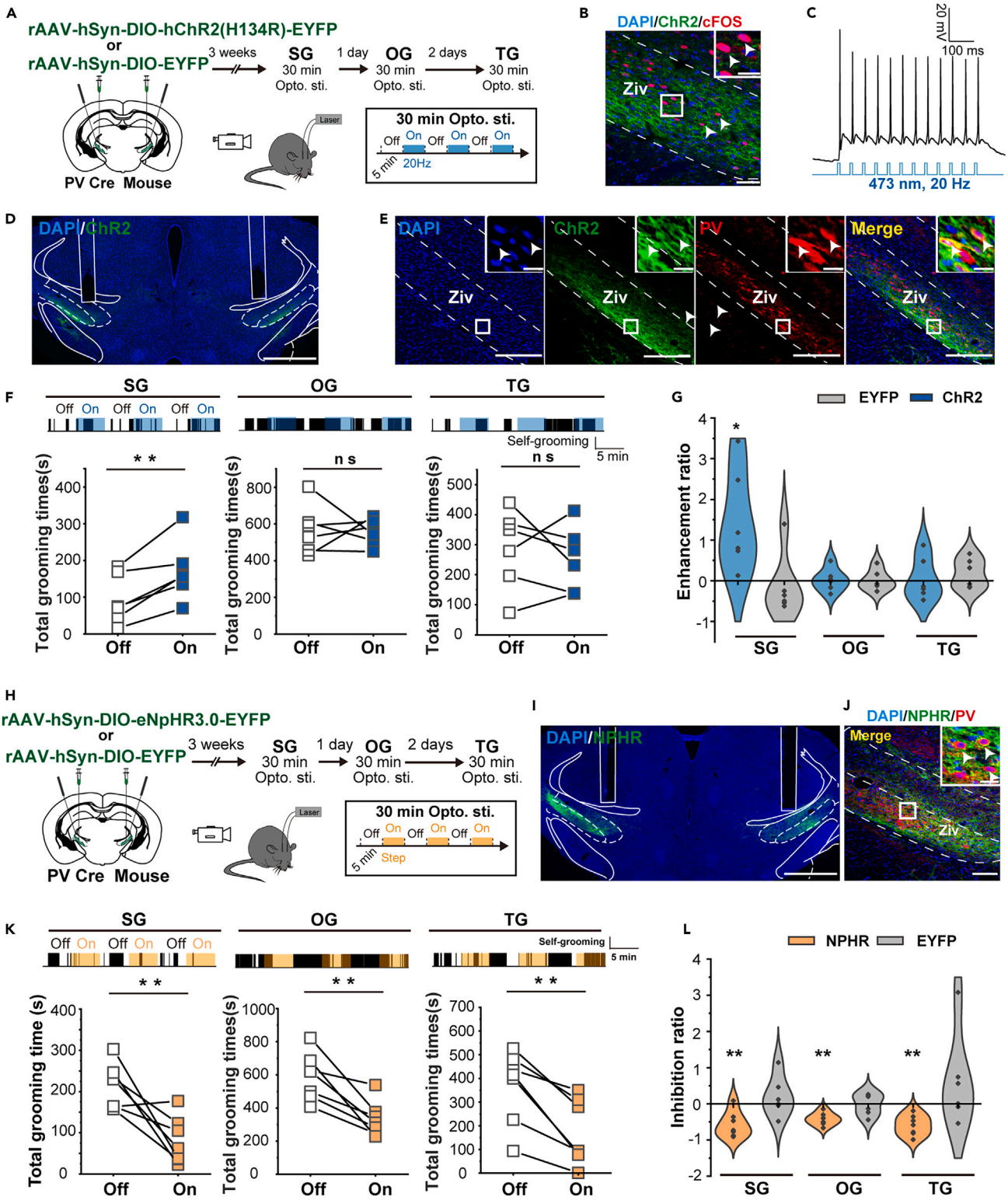

Figure 3. Activation of Ziv^{PV} neurons leads to increased spontaneous self-grooming

(A) Left, optogenetic activation of Ziv^{PV} neurons by targeting an optic fiber at Ziv that expressed ChR2-EYFP after injection with rAAV-hSyn-DIO-hChR2(H134R)-EYFP. Right, sequence of the self-grooming behavior test and the parameters of laser light.

(B) Representative images showing c-Fos protein (red) and ChR2-EYFP (green) in the Ziv. Scale bars for image and inset are 50 μm and 20 μm, respectively.

Figure 3. *Continued*

(C) Light-pulse trains (5 ms, 5 mW, 20 Hz) reliably evoked phase-locked spiking in ChR2-expressing Ziv^{PV} neurons in acute brain slices.

(D) Example coronal brain section showing the optical fiber track above the ChR2-expressing neurons in the Ziv of PV-IRES-Cre mice. Scale bar, 1 mm.

(E) Example micrographs from the Ziv showing colocalization of ChR2 (green) with PV protein (red). Scale bars for image and inset are 200 μm and 20 μm, respectively.

(F) Optical activation of Ziv^{PV} neurons increase spontaneous self-grooming, but not oil-induced self-grooming and tail suspension-induced self-grooming. Left, *two-tailed paired t test* ($n = 6$ mice): $t = -4.645$, $df = 5$, $p = 0.006$; Middle, *two-tailed paired t test* ($n = 6$ mice): $t = 0.196$, $df = 5$, $p = 0.853$; Right, *two-tailed paired t test* ($n = 6$ mice): $t = 0.649$, $df = 5$, $p = 0.545$. $^{**}p < 0.01$.

(G) The enhancement rate of self-grooming = (self-grooming $time_{on}$ – self-grooming $time_{off}$)/self-grooming $time_{off}$. *One-sample t test* ($n = 6$ mice in ChR2 group and 6 mice in the EYFP group): $t_{ChR2\ SG} = 2.876$, $df = 5$, $p = 0.035$; $t_{EYFP\ SG} = -0.463$, $df = 5$, $p = 0.663$; $t_{ChR2\ OG} = 0.199$, $df = 5$, $p = 0.85$; $t_{EYFP\ OG} = 0.126$, $df = 5$, $p = 0.905$; $t_{ChR2\ TG} = 0.196$, $df = 5$, $p = 0.852$; $t_{EYFP\ TG} = 1.235$, $df = 5$, $p = 0.272$.

(H) Left, optogenetic inhibition of Ziv^{PV} neurons by targeting an optic fiber at Ziv that expressed NPHR-EYFP after injection with rAAV-hSyn-DIO-eNpHR3.0-EYFP. Right, sequence of the self-grooming behavior test and the parameters of laser light.

(I) Example coronal brain section showing the optical fiber track above the NPHR-expressing neurons in the Ziv of PV-IRES-Cre mice. Scale bar, 1 mm.

(J) Example micrographs from the Ziv showing colocalization of NPHR (green) with PV protein (red). Scale bars for image and inset are 100 μm and 10 μm, respectively.

(K) Optical inhibition of Ziv PV + neurons suppress self-grooming. Left, *two-tailed paired t test* ($n = 7$ mice): $t = 3.686$, $df = 6$, $p = 0.01$; Middle, *two-tailed paired t test* ($n = 7$ mice): $t = 4.592$, $df = 6$, $p = 0.004$; Right, *two-tailed paired t test* ($n = 7$ mice): $t = 5.023$, $df = 6$, $p = 0.002$. $^{**}p < 0.01$.

(L) The inhibition rate of self-grooming = (self-grooming $time_{on}$ – self-grooming $time_{off}$)/self-grooming $time_{off}$. *One-sample t test* ($n = 7$ mice in NPHR group and 6 mice in the EYFP group): $t_{eNPHR\ SG} = -4.283$, $df = 6$, $p = 0.005$; $t_{EYFP\ SG} = 0.88$, $df = 5$, $p = 0.419$; $t_{eNPHR\ OG} = -6.53$, $df = 6$, $p = 0.001$; $t_{EYFP\ OG} = -0.161$, $df = 5$, $p = 0.879$; $t_{eNPHR\ TG} = -5.639$, $df = 6$, $p = 0.001$; $t_{EYFP\ TG} = 1.196$, $df = 5$, $p = 0.285$.

(Figure S5C). However, light delivery did not affect SG or TG (Figure 5H, left and right panels). We also injected rAAV-CaMKIIα-EYFP into the S1 and implanted an optical fiber onto the Ziv in the control group (Figure S5B). The results showed that light delivery did not affect SG, OG, or TG in the control group.

Furthermore, we injected rAAV2/Retro-hSyn-CRE-mCherry into the Ziv and rAAV-hSyn-DIO-hChR2(H134R)-EYFP or rAAV-hSyn-DIO-eNpHR3.0-EYFP into the S1, and an optical fiber was implanted onto the S1 to stimulate the pyramidal neurons projecting to the Ziv (Figure 5I). The results obtained were consistent with previous findings, demonstrating that activation of the $S1^{CaMKII} \rightarrow Ziv^{PV}$ pathway can increase SG in a natural state (Figure 5J). Inhibition of the S1→Ziv circuit was only necessary for OG, not for TG (Figure 5K), highlighting the specificity and necessity of the S1→Ziv circuit in sensory-evoked self-grooming. And the total grooming time changes are mostly explained by the average time of each bout (Figure S5D).

The $Cea^{SST} \rightarrow Ziv^{PV}$ circuit regulates stress-induced self-grooming and sensory-induced self-grooming

Finally, we investigated the functional connections of the $Cea^{SST} \rightarrow Ziv^{PV}$ pathway. To do this, we injected rAAV-DIO-hChR2(H134R)-mCherry into the CeA of SST-IRES-Cre mice (Figure 6A). After three weeks, we conducted whole-cell voltage-clamp recordings from cells in the Ziv to record ChR2-induced postsynaptic currents (Figure 6B, left panel). These recordings were performed in the presence of tetrodotoxin and 4-aminopyridine to exclude polysynaptic connections. By using an inhibitor of GABA receptors (bicuculline), we observed that bicuculline had a significant effect on synaptic responses (Figure 6B, middle and right panels), which is consistent with previous research.[46] Furthermore, we employed a similar strategy to investigate the role of the $Cea^{SST} \rightarrow Ziv^{PV}$ circuit in different types of grooming. We injected rAAV-DIO-hChR2(H134R)-EYFP (Figure 6C) or rAAV-DIO-mCherry (Figure S6E) into the CeA and implanted an optical fiber onto the Ziv for optogenetic stimulation of the inhibitory $Cea^{SST} \rightarrow Ziv^{PV}$ pathway terminals (Figure 6C). Interestingly, the activation of this pathway significantly increased all three types of grooming behavior (Figure 6D). Conversely, inhibition of the $Cea^{SST} \rightarrow Ziv^{PV}$ circuit did not have any effect on any of the three types of grooming behavior (Figures 6E and 6F). This may be related to the intricate local negative regulation in the Ziv, as indicated by the following pieces of evidence. First, rAAV-CaMKIIα-hChR2(H134R)-mCherry was administered into the S1 and rAAV-hSyn-DIO-hChR2(H134R)-EYFP was administered into the CeA of SST-IRES-Cre mice (Figure S6A), resulting in distinct fiber distributions within the Ziv, with mCherry fibers from the S1 predominantly located in the dorsal region and EYFP axons from the CeA predominantly located in the ventral region of the Ziv (Figure S6B). Subsequently, rAAV-hSyn-Flp was injected into the CeA, and rAAV-EFla-fDIO-EGFP was injected into the Ziv to label the PV neurons in the Ziv receiving CeA projections (Figure S6C), revealing that the neurons receiving CeA projections sent axons to the dorsal part of the Ziv (Figure S6D).

DISCUSSION

In the present study, our findings indicate that the Ziv serves as a potential integrative node for circuits involved in sensory-induced self-grooming and stress-induced self-grooming. First, the PV neurons in the Ziv not only positively regulate self-grooming behavior under normal physiological conditions but also regulate self-grooming behavior induced by sensory stimuli and stress. Second, glutamatergic inputs from the S1 region activate the Ziv and specifically contribute to OG, but not TG. Finally, GABAergic inputs from the CeA region inhibit the Ziv and participate in SG, OG, and TG, revealing the complex role of sensory and emotional information in self-grooming behavior.

Self-grooming behaviors can be broadly categorized into two types: sensation-induced self-grooming and stress-induced grooming. Previous studies have shown that mice exhibit extensive self-grooming when sprayed with water[14,15] or placed in a swimming pool.[15,47] However, these paradigms introduce stress to the mice through the action of spraying water or physical exertion during swimming. To minimize the

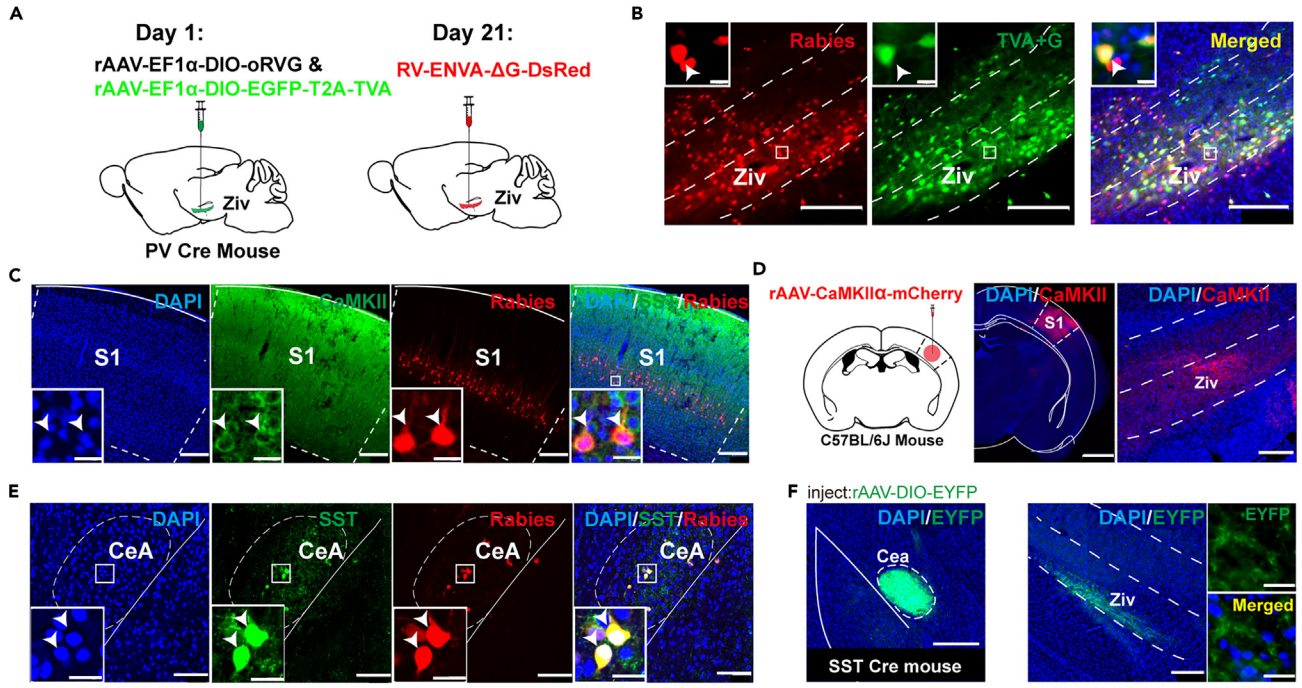

Figure 4. The presynaptic inputs to Ziv^{PV} neurons

(A) Schematic of the Cre-dependent retrograde *trans*-monosynaptic rabies virus tracing strategy.

(B) Typical images of injection sites and viral expression within the Ziv of PV-IRES-Cre mice. Starter cells (yellow) co-expressing rAAV-EF1α-DIO-EGFP-T2A-TVA, rAAV-EF1α-DIO-oRVG (green), and rabies RV-EnvA-ΔG-dsRed (red). Scale bars for image and inset are 200 μm and 10 μm, respectively.

(C) dsRed-labeled neurons within the S1 traced from the Ziv were colocalized with the CaMKII immunofluorescence. Scale bars for image and inset are 200 μm and 20 μm, respectively.

(D) Left, schematic diagram and example coronal brain section showing injection of rAAV-CaMKIIα-mCherry into the S1 of C57/BL6 mice. Scale bar, 1 mm. Right, example coronal brain section showing mCherry+ axonal projections of S1^{CaMKII} neurons in the Ziv. Scale bar, 200 μm.

(E) dsRed-labeled neurons within the CeA traced from the Ziv were colocalized with the SST immunofluorescence. Scale bars for image and inset are 100 μm and 20 μm, respectively.

(F) Left, schematic diagram and example coronal brain section showing injection of rAAV-hSyn-DIO-EYFP into the CeA of SST-IRES-Cre mice. Scale bar, 200 μm. Right, example coronal brain section showing EYFP+ axonal projections of Cea^{SST} neurons in the Ziv. Scale bar, 200 μm for the big image and 20 μm for blown-up images.

influence of stress on the induction of sensory-related grooming behaviors in mice, we applied corn oil to the orofacial area to induce stable sensory-dependent and stress-independent self-grooming.[12] Additionally, existing stress-induced self-grooming models, such as body restraint[15] and electric shock protocols,[12] have limitations, such as the presence of sensory factors or potential injury to the mouse's paws. In the present study, we developed a new stress-induced self-grooming model using tail suspension, which minimizes the influence of sensory factors. The utilization of these two models enables the distinction between the neural circuits involved in self-grooming induced by sensory stimuli and those induced by stress. We found that the Ziv was an important region involved in self-grooming behavior. While we acknowledge that activation of the Zid during OG (Figure 1F) suggests that the Zid may be involved in sensory input during self-grooming behavior, our study aimed to identify a potential site involved in both sensory input and stress input, leading us to focus on the Ziv rather than the Zid.

Previous studies have shown that the ZI, which is the ventral part of the thalamus, plays an important role in different innate behaviors through its innervation of different subregions and subsets of neurons.[31–35,48] The Ziv, located in the ventral part of the ZI, is involved in sensorimotor and emotional processes due to its widespread connectivity with various neural centers.[30,34–37,41,42] Although the regulation of innate behavior does not solely rely on the ZI, as this region also widely receives information from various upstream regions,[36,38] our findings still suggest that the Ziv may serve as a potential crucial node in integrating information related to self-grooming. Indeed, we demonstrated that the Ziv is necessary for self-grooming, as its inhibition suppressed SG, OG, and TG. However, activation of the Ziv led to an increase in spontaneous self-grooming, but not OG or TG. We suspected that the activation of the Ziv may reach a plateau in response to sensory or stressful stimuli in the present models. The self-grooming levels in the OG and TG groups were greater than those in the SG group during the off stage of optogenetics (Figure 3F). Consequently, the optogenetic stimulation of the Ziv^{PV} neurons may not have induced additional elevations in self-grooming levels within the OG and TG groups.

The identification of the projections of Ziv^{PV} neurons provides insights into how the Ziv coordinates with the S1 and CeA regions to generate different types of self-grooming motor actions. Previous studies have shown that the S1 has excitatory effects on the Ziv,[35] while the CeA has inhibitory effects on the Ziv.[46] Our results support these findings and suggest that these two circuits may project to different

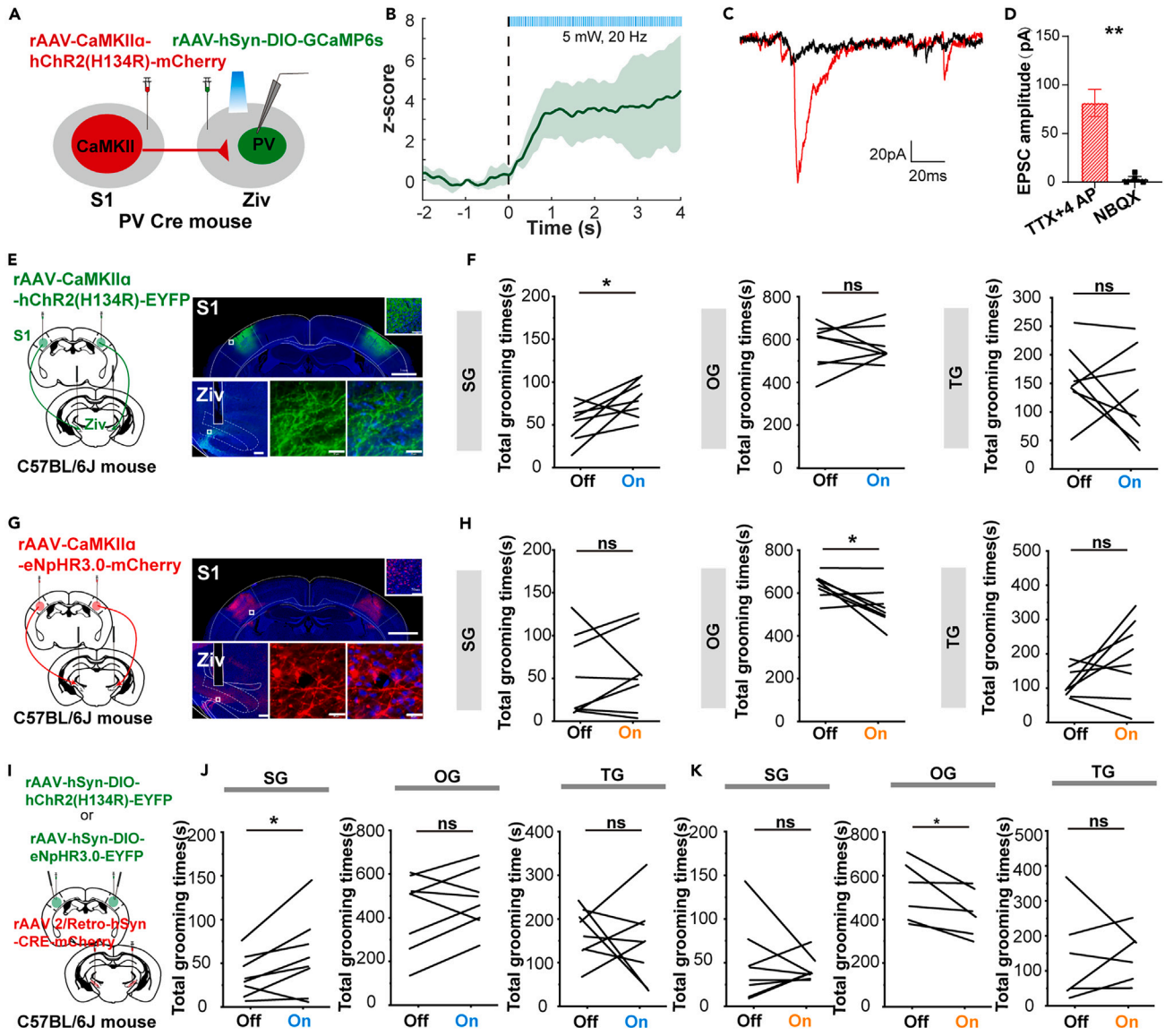

Figure 5. Activation and inhibition of the S1→Ziv circuit regulates self-grooming

(A) Left, schematics for simultaneous activation and recording cells *in vivo*, which was achieved by injection of rAAV-CaMKIIα-hChR2(H134R)-mCherry into S1 and the rAAV-hSyn-DIO-GCaMP6s was injected into Ziv in PV-IRES-Cre mouse.

(B) Averaged results of calcium activity in Ziv PV + neurons around the start of blue light were delivered into S1 (n = 28 trials from 3 mice).

(C and D) Representative traces (C) and summarized data (D) of light-evoked currents (473 nm, 20 Hz, 5ms) before and after 1,2,3,4-tetrahydro-6-nitro-2,3-dioxo (NBQX) (10 μM, n = 4 neurons from 2 mice). *Two-tailed unpaired t test* (n = 4 cells): t = 5.534, df = 6, p = 0.001. ***$p \leq 0.001$. Data are represented as mean ± SEM.

(E) Schematics for optogenetics manipulation. Targeted functional activation of the S1→Ziv circuitry was achieved by injection of rAAV-CaMKIIα-hChR2(H134R)-EYFP into S1, and implantation of optical fiber onto Ziv. Scale bars for image and inset are 1mm and 50 μm, respectively; scale bars for image and magnified images are 200 μm and 20 μm, respectively.

(F) Optogenetic stimulation of the terminals of the excitatory S1→Ziv pathway increased spontaneous self-grooming. Left, *two-tailed paired t test* (n = 8 mice): t = −2.698, df = 7, p = 0.031; Middle, *two-tailed paired t test* (n = 8 mice): t = −0.047, df = 7, p = 0.964; Right, *two-tailed paired t test* (n = 8 mice): t = 0.915, df = 7, p = 0.39. *p < 0.05.

(G) Schematics for optogenetics manipulation. Targeted functional inhibition of the S1→Ziv circuitry was achieved by injection of rAAV-CaMKIIα-eNpHR3.0-mCherry into S1 (A), and implantation of optical fiber onto Ziv (B). Scale bars for image and inset are 1 mm and 50 μm, respectively; scale bars for image and magnified images are 200 μm and 20 μm, respectively.

(H) Inhibition of the terminals of the excitatory S1→Ziv pathway decreased oil-induced self-grooming. Left, *two-tailed paired t test* (n = 8 mice): t = −0.386, df = 7, p = 0.711; Middle, *two-tailed paired t test* (n = 8 mice): t = 2.834, df = 7, p = 0.025; Right, *two-tailed paired t test* (n = 8 mice): t = −1.763, df = 7, p = 0.121. *p < 0.05.

(I) Schematics for optogenetics manipulation. Targeted functional activation of the S1→Ziv circuitry was achieved by injection of rAAV2/Retro-hSyn-Cre into Ziv, rAAV-hSyn-DIO-hChR2(H134R)-EYFP or rAAV-hSyn-DIO-eNpHR3.0-EYFP into S1 and implantation of optical fiber onto S1.

Figure 5. *Continued*

(J) The self-grooming time were significantly increased when light was delivered. Left, *two-tailed paired t test* ($n = 8$ mice): $t = -2.519$, $df = 7$, $p = 0.04$; Middle, *two-tailed paired t test* ($n = 8$ mice): $t = -1.252$, $df = 7$, $p = 0.251$; Right, *two-tailed paired t test* ($n = 8$ mice): $t = 0.466$, $df = 7$, $p = 0.655$. $^*p < 0.05$.

(K) The oil-induced self-grooming time were significantly decreased when light was delivered. Left, *Wilcoxon signed-rank test* ($n = 8$ mice): $Z = -0.169$, $p = 0.866$; Middle, *two-tailed paired t test* ($n = 6$ mice): $t = 2.673$, $df = 5$, $p = 0.044$; Right, *two-tailed paired t test* ($n = 6$ mice): $t = -0.165$, $df = 5$, $p = 0.876$. $^*p < 0.05$.

groups of PV neurons in the Ziv (Figures S6A and S6B). Furthermore, we revealed that glutamatergic inputs from the primary sensory cortex (S1) are activated in the Ziv and specifically contribute to OG. Conversely, optogenetic activation of GABAergic inputs from the CeA to the Ziv increased SG, OG, and TG, potentially due to the complex local negative regulation within the Ziv. First, our results indicated that the axons originating from the S1 projected to the dorsal region of the Ziv, while the axons from the CeA targeted the ventral region of the Ziv (Figures S6A and S6B). Additionally, through the use of an AAV1 anterograde transsynaptic strategy and the flippase (Flp) dependent fashion (Flp-fDIO) method, we found that neurons receiving projections from the CeA may project to the dorsal part of the Ziv (Figures S6C and S6D). Notably, when we activated the axons from the S1 and suppressed the axons from the CeA in the Ziv, the neuronal activity in the Ziv exhibited a smaller increase than did the activation of the S1 projections to the Ziv (data not shown here). These results suggested that PV neurons receiving inhibitory projections from the CeA concurrently inhibit PV neurons receiving excitatory S1 projections in the Ziv. This negative modulation within the Ziv may play a role in the intricate sensory and emotional interactions involved in self-grooming behavior.

According to our results, the $S1^{CaMKII} \rightarrow Ziv^{PV}$ pathway primarily focuses on sensory information during self-grooming. The $Cea^{SST} \rightarrow Ziv^{PV}$ pathway may be involved in the complex local negative regulation of the ZI region and the integration of sensory and emotional information in self-grooming behavior. It is worth noting that rodents exhibiting increased self-grooming behavior also frequently display anxiety-like behavior[7,11,19] and sensory abnormalities,[12,49] suggesting a potential interaction between sensory and emotional information in repetitive self-grooming.[12] In this context, the act of stress-induced self-grooming itself generates new sensory stimuli to the face, while sensory-induced repetitive self-grooming may generate new stress stimuli. Our findings highlight the Ziv region as a key player in processing sensory and emotional information related to self-grooming, as well as its upward information intake. These findings may offer new targets for the treatment of stereotyped behavior and provide insights into the interplay between emotions and self-grooming behavior.

Limitation of the study

However, our study has certain limitations. For example, we cannot entirely rule out the possibility that the activation of the CeA projection to the Ziv could activate other postsynaptic regions to the CeA through antidromic collaterals. Further direct evidence is needed to substantiate the local negative network modulation in the Ziv by the CeA and S1. Employing a method to simultaneously express dual colorful GCaMP proteins in these two neuron populations and imaging them could serve as a means to validate this hypothesis in subsequent investigations. In addition, self-grooming has a well-preserved sequence pattern[50]; however, we did not extensively focus on the circuitry mechanisms underlying the grooming microstructure.

STAR★METHODS

Detailed methods are provided in the online version of this paper and include the following:

- KEY RESOURCES TABLE
- RESOURCE AVAILABILITY
  - Lead contact
  - Materials availability
  - Data and code availability
- EXPERIMENTAL MODEL AND STUDY PARTICIPANT DETAILS
- METHOD DETAILS
  - Virus and trace injection
  - Optogenetic manipulation
  - Grooming behavioral test
  - Fiber photometry
  - Brain slice electrophysiology and optogenetics
  - Immunohistochemistry
- QUANTIFICATION AND STATISTICAL ANALYSIS

SUPPLEMENTAL INFORMATION

Supplemental information can be found online at https://doi.org/10.1016/j.isci.2024.110165.

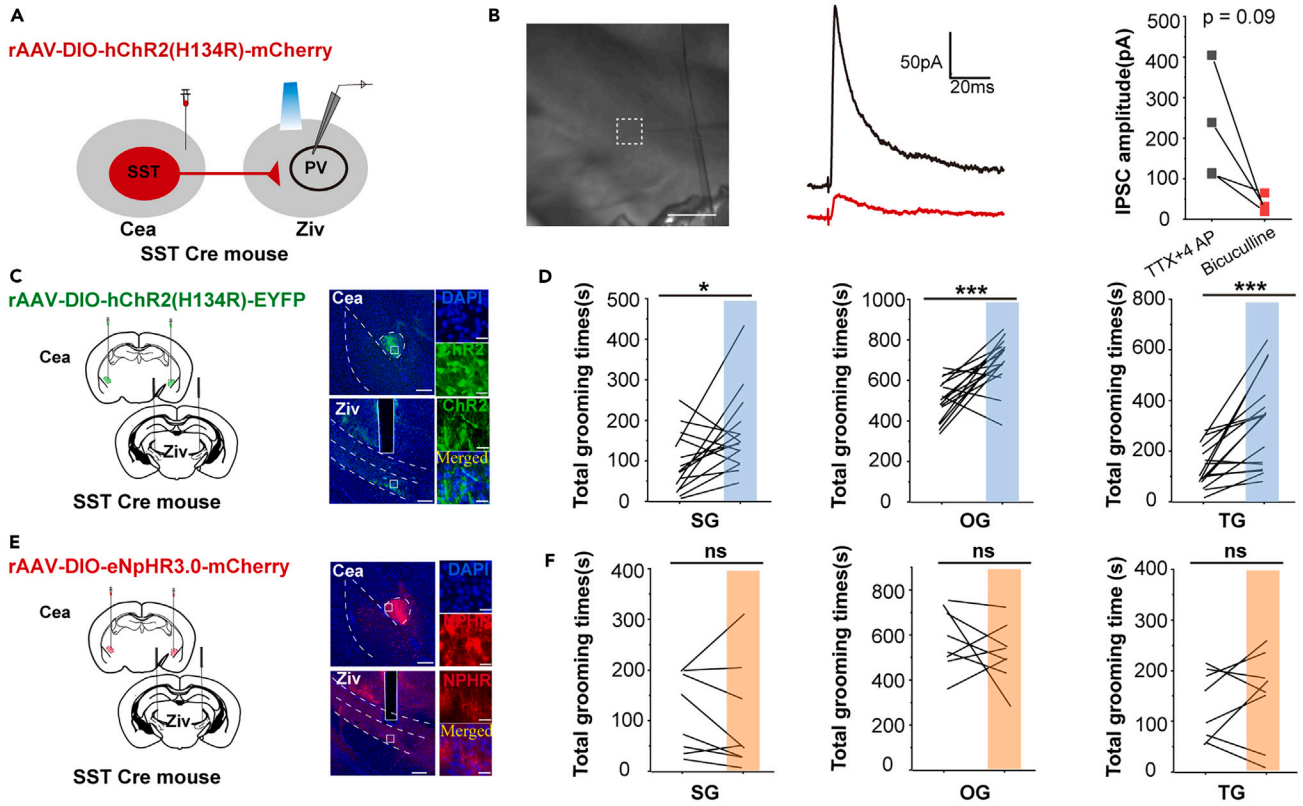

Figure 6. Activation and inhibition of the Cea→Ziv circuit regulates self-grooming

(A) Schematics for simultaneous activation and recording cells *in vivo*, which was achieved by injection of rAAV -DIO-hChR2(H134R)-mCherry into Cea in SST-IRES-Cre mouse.

(B) Left, schematic of recording configuration in acute slices. Representative traces (middle) and summarized data (right) of light-evoked currents (473 nm, 20 Hz, 5ms) before and after Bicuculline (50 μM, $n = 4$ neurons from 4 mice). *Two-tailed paired t test* ($n = 4$ cells): $t = 2.448$, $df = 3$, $p = 0.09$. Scale bar, 200 μm.

(C) Schematics for optogenetics manipulation. Targeted functional activation of the CeA→Ziv circuitry was achieved by injection of rAAV-DIO-hChR2(H134R)-EYFP into CeA, and implantation of optical fiber onto Ziv. Scale bars for image and magnified images are 200 μm and 20 μm, respectively.

(D) Optogenetic stimulation of the terminals of the inhibitory CeA→Ziv pathway increased all types self-grooming. Left, *Wilcoxon signed-rank test* ($n = 15$ mice): $Z = -1.988$, $p = 0.047$; Middle, *two-tailed paired t test* ($n = 16$ mice): $t = -4.405$, $df = 15$, $p = 0.001$; Right, *two-tailed paired t test* ($n = 16$ mice): $t = -4.312$, $df = 15$, $p = 0.001$. $^{*}p < 0.05$, $^{***}p \leq 0.001$.

(E) Schematics for optogenetics manipulation. Targeted functional activation of the CeA→Ziv circuitry was achieved by injection of rAAV-DIO-eNpHR3.0-mCherry into CeA, and implantation of optical fiber onto Ziv. Scale bars for image and magnified images are 200 μm and 20 μm, respectively.

(F) Optogenetic stimulation of the terminals of the inhibitory CeA→Ziv pathway did not worked for any types self-grooming. *Wilcoxon signed-rank test* ($n = 8$ mice): $Z = -0.980$, $p = 0.327$; Middle, *two-tailed paired t test* ($n = 8$ mice): $t = 0.893$, $df = 7$, $p = 0.401$; Right, *two-tailed paired t test* ($n = 8$ mice): $t = -0.767$, $df = 7$, $p = 0.468$.

ACKNOWLEDGMENTS

This study was supported by STI2030-Major Project of China (2021ZD0201005 to S.W.), Natural Science Foundation of China (82271577, 82071536 to W.W., 82221001 to S.W., and 82371236 to Y.Z.), Shaanxi Provincial Innovation Chain Project of Key Industries (2023-ZDLSF-47 to W.W.), and Key Research and Development Program of Shaanxi Province (2023-YBSF-106 to Q.X., 2020SF-127 to Q.X.). We thank American Journal Experts for English language editing (certificate verification code: 9BC9-2109-29D1-081E-E6B8).

AUTHOR CONTRIBUTIONS

W.W. and Q.X. contributed to experimental design and discussion. J.G., P.R., B.T., J.L., Q.H., C.Q., and K.R. performed the experiments and collected data. J.G., P.R., B.T., J.L., E.H., and H.M. analyzed data. J.G., W.W., Q.X., S.W., and Y.Z. wrote, edited, and reviewed the manuscript. All authors read and approved the final manuscript.

DECLARATION OF INTERESTS

The authors declare no competing interests.

Received: October 28, 2023
Revised: April 12, 2024
Accepted: May 29, 2024
Published: June 3, 2024

REFERENCES

1. Kalueff, A.V., Stewart, A.M., Song, C., Berridge, K.C., Graybiel, A.M., and Fentress, J.C. (2016). Neurobiology of rodent self-grooming and its value for translational neuroscience. Nat. Rev. Neurosci. *17*, 45–59. https://doi.org/10.1038/nrn.2015.8.
2. Spruijt, B.M., van Hooff, J.A., and Gispen, W.H. (1992). Ethology and neurobiology of grooming behavior. Physiol. Rev. *72*, 825–852. https://doi.org/10.1152/physrev.1992.72.3.825.
3. Zhang, Y.F., Janke, E., Bhattarai, J.P., Wesson, D.W., and Ma, M. (2022). Self-directed orofacial grooming promotes social attraction in mice via chemosensory communication. iScience *25*, 104284. https://doi.org/10.1016/j.isci.2022.104284.
4. Ramírez-Armenta, K.I., Alatriste-Leon, H., Verma-Rodriguez, A.K., Llanos-Moreno, A., Ramirez-Jarquin, J.O., and Tecuapetla, F. (2022). Optogenetic inhibition of indirect pathway neurons in the dorsomedial striatum reduces excessive grooming in Sapap3-knockout mice. Neuropsychopharmacology *47*, 477–487. https://doi.org/10.1038/s41386-021-01161-9.
5. Welch, J.M., Lu, J., Rodriguiz, R.M., Trotta, N.C., Peca, J., Ding, J.D., Feliciano, C., Chen, M., Adams, J.P., Luo, J., et al. (2007). Cortico-striatal synaptic defects and OCD-like behaviours in Sapap3-mutant mice. Nature *448*, 894–900. https://doi.org/10.1038/nature06104.
6. Monteiro, P., and Feng, G. (2017). SHANK proteins: roles at the synapse and in autism spectrum disorder. Nat. Rev. Neurosci. *18*, 147–157. https://doi.org/10.1038/nrn.2016.183.
7. Guo, B., Chen, J., Chen, Q., Ren, K., Feng, D., Mao, H., Yao, H., Yang, J., Liu, H., Liu, Y., et al. (2019). Anterior cingulate cortex dysfunction underlies social deficits in Shank3 mutant mice. Nat. Neurosci. *22*, 1223–1234. https://doi.org/10.1038/s41593-019-0445-9.
8. McFarlane, H.G., Kusek, G.K., Yang, M., Phoenix, J.L., Bolivar, V.J., and Crawley, J.N. (2008). Autism-like behavioral phenotypes in BTBR T+tf/J mice. Gene Brain Behav. *7*, 152–163. https://doi.org/10.1111/j.1601-183X.2007.00330.x.
9. Schwartzer, J.J., Careaga, M., Onore, C.E., Rushakoff, J.A., Berman, R.F., and Ashwood, P. (2013). Maternal immune activation and strain specific interactions in the development of autism-like behaviors in mice. Transl. Psychiatry *3*, e240. https://doi.org/10.1038/tp.2013.16.
10. Wang, B., Zheng, Y., Shi, H., Du, X., Zhang, Y., Wei, B., Luo, M., Wang, H., Wu, X., Hua, X., et al. (2017). Zfp462 deficiency causes anxiety-like behaviors with excessive self-grooming in mice. Gene Brain Behav. *16*, 296–307. https://doi.org/10.1111/gbb.12339.
11. Liu, H., Huang, X., Xu, J., Mao, H., Li, Y., Ren, K., Ma, G., Xue, Q., Tao, H., Wu, S., and Wang, W. (2021). Dissection of the relationship between anxiety and stereotyped self-grooming using the Shank3B mutant autistic model, acute stress model and chronic pain model. Neurobiol. Stress *15*, 100417. https://doi.org/10.1016/j.ynstr.2021.100417.
12. Xie, Z., Li, D., Cheng, X., Pei, Q., Gu, H., Tao, T., Huang, M., Shang, C., Geng, D., Zhao, M., et al. (2022). A brain-to-spinal sensorimotor loop for repetitive self-grooming. Neuron *110*, 874–890.e7. https://doi.org/10.1016/j.neuron.2021.11.028.
13. Pelissier, T., Pajot, J., and Dallel, R. (2002). The orofacial capsaicin test in rats: effects of different capsaicin concentrations and morphine. Pain *96*, 81–87. https://doi.org/10.1016/s0304-3959(01)00432-8.
14. Hill, R.A., McInnes, K.J., Gong, E.C.H., Jones, M.E.E., Simpson, E.R., and Boon, W.C. (2007). Estrogen deficient male mice develop compulsive behavior. Biol. Psychiatr. *61*, 359–366. https://doi.org/10.1016/j.biopsych.2006.01.012.
15. Mu, M.D., Geng, H.Y., Rong, K.L., Peng, R.C., Wang, S.T., Geng, L.T., Qian, Z.M., Yung, W.H., and Ke, Y. (2020). A limbic circuitry involved in emotional stress-induced grooming. Nat. Commun. *11*, 2261. https://doi.org/10.1038/s41467-020-16203-x.
16. Sun, J., Yuan, Y., Wu, X., Liu, A., Wang, J., Yang, S., Liu, B., Kong, Y., Wang, L., Zhang, K., et al. (2022). Excitatory SST neurons in the medial paralemniscal nucleus control repetitive self-grooming and encode reward. Neuron *110*, 3356–3373.e8. https://doi.org/10.1016/j.neuron.2022.08.010.
17. Füzesi, T., Daviu, N., Wamsteeker Cusulin, J.I., Bonin, R.P., and Bains, J.S. (2016). Hypothalamic CRH neurons orchestrate complex behaviours after stress. Nat. Commun. *7*, 11937. https://doi.org/10.1038/ncomms11937.
18. Langen, M., Kas, M.J.H., Staal, W.G., van Engeland, H., and Durston, S. (2011). The neurobiology of repetitive behavior: of mice. Neurosci. Biobehav. Rev. *35*, 345–355. https://doi.org/10.1016/j.neubiorev.2010.02.004.
19. Song, C., Berridge, K.C., and Kalueff, A.V. (2016). Stressing' rodent self-grooming for neuroscience research. Nat. Rev. Neurosci. *17*, 591. https://doi.org/10.1038/nrn.2016.103.
20. Wang, W., Li, C., Chen, Q., van der Goes, M.S., Hawrot, J., Yao, A.Y., Gao, X., Lu, C., Zang, Y., Zhang, Q., et al. (2017). Striatopallidal dysfunction underlies repetitive behavior in Shank3-deficient model of autism. J. Clin. Invest. *127*, 1978–1990. https://doi.org/10.1172/jci87997.
21. Peça, J., Feliciano, C., Ting, J.T., Wang, W., Wells, M.F., Venkatraman, T.N., Lascola, C.D., Fu, Z., and Feng, G. (2011). Shank3 mutant mice display autistic-like behaviours and striatal dysfunction. Nature *472*, 437–442. https://doi.org/10.1038/nature09965.
22. Cromwell, H.C., and Berridge, K.C. (1996). Implementation of action sequences by a neostriatal site: a lesion mapping study of grooming syntax. J. Neurosci. *16*, 3444–3458. https://doi.org/10.1523/jneurosci.16-10-03444.1996.
23. Graybiel, A.M., and Grafton, S.T. (2015). The striatum: where skills and habits meet. Cold Spring Harbor Perspect. Biol. *7*, a021691. https://doi.org/10.1101/cshperspect.a021691.
24. Berridge, K.C., and Whishaw, I.Q. (1992). Cortex, striatum and cerebellum: control of serial order in a grooming sequence. Exp. Brain Res. *90*, 275–290. https://doi.org/10.1007/BF00227239.
25. Watson, P.J. (1978). Behavior maintained by electrical stimulation of the rat cerebellum. Physiol. Behav. *21*, 749–755. https://doi.org/10.1016/0031-9384(78)90014-8.
26. Hong, W., Kim, D.W., and Anderson, D.J. (2014). Antagonistic control of social versus repetitive self-grooming behaviors by separable amygdala neuronal subsets. Cell *158*, 1348–1361. https://doi.org/10.1016/j.cell.2014.07.049.
27. Mangieri, L.R., Lu, Y., Xu, Y., Cassidy, R.M., Xu, Y., Arenkiel, B.R., and Tong, Q. (2018). A neural basis for antagonistic control of feeding and compulsive behaviors. Nat. Commun. *9*, 52. https://doi.org/10.1038/s41467-017-02534-9.
28. Xu, Y., Lu, Y., Cassidy, R.M., Mangieri, L.R., Zhu, C., Huang, X., Jiang, Z., Justice, N.J., Xu, Y., Arenkiel, B.R., and Tong, Q. (2019). Identification of a neurocircuit underlying regulation of feeding by stress-related emotional responses. Nat. Commun. *10*, 3446. https://doi.org/10.1038/s41467-019-11399-z.
29. Islam, M.T., Maejima, T., Matsui, A., and Mieda, M. (2022). Paraventricular hypothalamic vasopressin neurons induce self-grooming in mice. Mol. Brain *15*, 47. https://doi.org/10.1186/s13041-022-00932-9.
30. Yang, Y., Jiang, T., Jia, X., Yuan, J., Li, X., and Gong, H. (2022). Whole-Brain Connectome of GABAergic Neurons in the Mouse Zona Incerta. Neurosci. Bull. *38*, 1315–1329. https://doi.org/10.1007/s12264-022-00930-w.
31. Zhang, X., and van den Pol, A.N. (2017). Rapid binge-like eating and body weight gain driven by zona incerta GABA neuron activation. Science *356*, 853–859. https://doi.org/10.1126/science.aam7100.
32. Liu, K., Kim, J., Kim, D.W., Zhang, Y.S., Bao, H., Denaxa, M., Lim, S.A., Kim, E., Liu, C., Wickersham, I.R., et al. (2017). Lhx6-positive GABA-releasing neurons of the zona incerta promote sleep. Nature *548*, 582–587. https://doi.org/10.1038/nature23663.
33. Shang, C., Liu, A., Li, D., Xie, Z., Chen, Z., Huang, M., Li, Y., Wang, Y., Shen, W.L., and Cao, P. (2019). A subcortical excitatory circuit for sensory-triggered predatory hunting in mice. Nat. Neurosci. *22*, 909–920. https://doi.org/10.1038/s41593-019-0405-4.
34. Zhao, Z.D., Chen, Z., Xiang, X., Hu, M., Xie, H., Jia, X., Cai, F., Cui, Y., Chen, Z., Qian, L., et al. (2019). Zona incerta GABAergic neurons integrate prey-related sensory signals and induce an appetitive drive to promote hunting. Nat. Neurosci. *22*, 921–932. https://doi.org/10.1038/s41593-019-0404-5.

35. Wang, X., Chou, X., Peng, B., Shen, L., Huang, J.J., Zhang, L.I., and Tao, H.W. (2019). A cross-modality enhancement of defensive flight via parvalbumin neurons in zona incerta. Elife *8*, e42728. https://doi.org/10.7554/eLife.42728.
36. Ahmadlou, M., Houba, J.H.W., van Vierbergen, J.F.M., Giannouli, M., Gimenez, G.A., van Weeghel, C., Darbanfouladi, M., Shirazi, M.Y., Dziubek, J., Kacem, M., et al. (2021). A cell type-specific cortico-subcortical brain circuit for investigatory and novelty-seeking behavior. Science *372*, eabe9681. https://doi.org/10.1126/science.abe9681.
37. Ogasawara, T., Sogukpinar, F., Zhang, K., Feng, Y.Y., Pai, J., Jezzini, A., and Monosov, I.E. (2022). A primate temporal cortex-zona incerta pathway for novelty seeking. Nat. Neurosci. *25*, 50–60. https://doi.org/10.1038/s41593-021-00950-1.
38. Wang, H., Dong, P., He, C., Feng, X.Y., Huang, Y., Yang, W.W., Gao, H.J., Shen, X.F., Lin, S., Cao, S.X., et al. (2020). Incerta-thalamic Circuit Controls Nocifensive Behavior via Cannabinoid Type 1 Receptors. Neuron *107*, 538–551.e7. https://doi.org/10.1016/j.neuron.2020.04.027.
39. Hu, T.T., Wang, R.R., Du, Y., Guo, F., Wu, Y.X., Wang, Y., Wang, S., Li, X.Y., Zhang, S.H., and Chen, Z. (2019). Activation of the Intrinsic Pain Inhibitory Circuit from the Midcingulate Cg2 to Zona Incerta Alleviates Neuropathic Pain. J. Neurosci. *39*, 9130–9144. https://doi.org/10.1523/JNEUROSCI.1683-19.2019.
40. Masri, R., Quiton, R.L., Lucas, J.M., Murray, P.D., Thompson, S.M., and Keller, A. (2009). Zona incerta: a role in central pain. J. Neurophysiol. *102*, 181–191. https://doi.org/10.1152/jn.00152.2009.
41. Li, J., Bai, Y., Liang, Y., Zhang, Y., Zhao, Q., Ge, J., Li, D., Zhu, Y., Cai, G., Tao, H., et al. (2022). Parvalbumin Neurons in Zona Incerta Regulate Itch in Mice. Front. Mol. Neurosci. *15*, 843754. https://doi.org/10.3389/fnmol.2022.843754.
42. Kolmac, C., and Mitrofanis, J. (1999). Distribution of various neurochemicals within the zona incerta: an immunocytochemical and histochemical study. Anat. Embryol. *199*, 265–280. https://doi.org/10.1007/s004290050227.
43. Zhu, X., Zhou, W., Jin, Y., Tang, H., Cao, P., Mao, Y., Xie, W., Zhang, X., Zhao, F., Luo, M.H., et al. (2019). A Central Amygdala Input to the Parafascicular Nucleus Controls Comorbid Pain in Depression. Cell Rep. *29*, 3847–3858.e5. https://doi.org/10.1016/j.celrep.2019.11.003.
44. Gilpin, N.W., Herman, M.A., and Roberto, M. (2015). The central amygdala as an integrative hub for anxiety and alcohol use disorders. Biol. Psychiatr. *77*, 859–869. https://doi.org/10.1016/j.biopsych.2014.09.008.
45. Wahis, J., Baudon, A., Althammer, F., Kerspern, D., Goyon, S., Hagiwara, D., Lefevre, A., Barteczko, L., Boury-Jamot, B., Bellanger, B., et al. (2021). Astrocytes mediate the effect of oxytocin in the central amygdala on neuronal activity and affective states in rodents. Nat. Neurosci. *24*, 529–541. https://doi.org/10.1038/s41593-021-00800-0.
46. Zhou, M., Liu, Z., Melin, M.D., Ng, Y.H., Xu, W., and Südhof, T.C. (2018). A central amygdala to zona incerta projection is required for acquisition and remote recall of conditioned fear memory. Nat. Neurosci. *21*, 1515–1519. https://doi.org/10.1038/s41593-018-0248-4.
47. Chesher, G.B., and Jackson, D.M. (1981). Swim-induced grooming in mice is mediated by a dopaminergic substrate. J. Neural. Transm. *50*, 47–55. https://doi.org/10.1007/BF01254913.
48. Venkataraman, A., Brody, N., Reddi, P., Guo, J., Gordon Rainnie, D., and Dias, B.G. (2019). Modulation of fear generalization by the zona incerta. Proc. Natl. Acad. Sci. USA *116*, 9072–9077. https://doi.org/10.1073/pnas.1820541116.
49. Chen, Q., Deister, C.A., Gao, X., Guo, B., Lynn-Jones, T., Chen, N., Wells, M.F., Liu, R., Goard, M.J., Dimidschstein, J., et al. (2020). Dysfunction of cortical GABAergic neurons leads to sensory hyper-reactivity in a Shank3 mouse model of ASD. Nat. Neurosci. *23*, 520–532. https://doi.org/10.1038/s41593-020-0598-6.
50. Kalueff, A.V., Aldridge, J.W., LaPorte, J.L., Murphy, D.L., and Tuohimaa, P. (2007). Analyzing grooming microstructure in neurobehavioral experiments. Nat. Protoc. *2*, 2538–2544. https://doi.org/10.1038/nprot.2007.367.
51. Friard, O., and Gamba, M. (2016). BORIS: a free, versatile open-source event-logging software for video/audio coding and live observations. Methods Ecol. Evol. *7*, 1325–1330. https://doi.org/10.1111/2041-210x.12584.
52. Li, Y., Zhong, W., Wang, D., Feng, Q., Liu, Z., Zhou, J., Jia, C., Hu, F., Zeng, J., Guo, Q., et al. (2016). Serotonin neurons in the dorsal raphe nucleus encode reward signals. Nat. Commun. *7*, 10503. https://doi.org/10.1038/ncomms10503.
53. Ting, J.T., Daigle, T.L., Chen, Q., and Feng, G. (2014). Acute brain slice methods for adult and aging animals: application of targeted patch clamp analysis and optogenetics. Methods Mol. Biol. *1183*, 221–242. https://doi.org/10.1007/978-1-4939-1096-0_14.

STAR★METHODS

KEY RESOURCES TABLE

REAGENT or RESOURCE	SOURCE	IDENTIFIER
Antibodies		
Rabbit monoclonal anti-cFOS (1:1000)	Synaptic System	Sysy-226008; RRID: AB_2891278
Rabbit polyclonal anti-PV (1:200)	GeneTex	Cat#GTX134110; RRID: AB_2887219
Rabbit polyclonal anti-CaMKII (1:1000)	Abcam	Cat#ab5683; RRID: AB_305050
Alexa 488-conjugated secondary antibody (1:500)	Invitrogen	Cat#A21206; RRID: AB_2535792
Rabbit polyclonal anti-SST (1:1000)	Immunostar	Cat#20067; RRID: AB_572264
Alexa 594-conjugated secondary antibody (1:500)	Invitrogen	Cat#A21207; RRID: AB_141637
Bacterial and virus strains		
rAAV-CaMKIIα-hChR2(H134R)-EYFP-WPRE-pA (5.04E + 12 gc/ml)	BrainVTA	Cat# PT-0296
rAAV-CaMKIIα-eNpHR3.0-EYFP-WPRE-pA (4.98E + 12 gc/ml)	BrainVTA	Cat# PT-0008
rAAV-CaMKIIα-hChR2(H134R)-mCherry-WPRE-pA (5.18E + 12 gc/ml)	BrainVTA	Cat# PT-0297
rAAV-hSyn-DIO-GCaMP6s-WPRE-pA (2.60E + 12 gc/ml)	BrainCase	Cat# BC-0238
rAAV-hSyn-DIO-hChR2(H134R)-EYFP-WPRE-pA (3.20E + 12 gc/ml)	BrainCase	Cat# BC-0107
rAAV- hSyn-DIO-eNpHR3.0-EYFP-WPRE-pA (2.41E + 12 gc/ml)	BrainVTA	Cat# PT-0006
AAV2/Retro-hSyn-CRE-mCherry-WPRE-hGH pA (1.20E + 13 gc/ml)	BrainVTA	Cat# PT-0407
rAAV- hSyn-DIO-EYFP-WPRE-bGH pA (2.5E + 12 gc/ml)	BrainVTA	Cat# PT-0795
rAAV-CaMKIIα-mCherry-WPRE-bGH pA (3.15E + 12 gc/ml)	BrainVTA	Cat# PT-0108
rAAV-EF1α-DIO-oRVG-WPRE-hGH-pA (3.87E + 12 gc/ml)	BrainVTA	Cat# PT-0023
rAAV-EF1α-DIO-EGFP-T2A-TVA-WPRE-hGH-pA (2.46E + 12 gc/ml)	BrainVTA	Cat# PT-0062
RV-ENVA-ΔG-DsRed (5.84E + 12 gc/ml)	BrainVTA	Cat# R01002
rAAV-hSyn-mCherry-WPRE-hGH-pA (5.11E + 12 gc/ml)	BrainVTA	Cat# PT-0100
rAAV-hSyn-eNpHR3.0-EYFP-WPRE-pA (5.62E + 12 gc/ml)	BrainVTA	Cat# PT-0010
rAAV-hSyn-Flp-WPRE-hGH (1.01E + 13 gc/ml)	BrainVTA	Cat# PT-0341
rAAV-EF1α-fDIO-EGFP-WPRE-hGH-pA (5.84E + 12 gc/ml)	BrainVTA	Cat# PT-1047
Chemicals, peptides, and recombinant proteins		
TTX	Taizhou Kangte Biology Co. , Ltd.	Cat#: TTX-99-L-1
4 AP	Tocris	Cat#: 0940
NBQX disodium salt	Tocris	Cat#: 1044
Bicuculline	Selleck	Cat#: S7071
Experimental models: Organisms/strains		
Mouse: wild type C57BL/6J	Charles river	Cat#: 219
Mouse: PV-IRES-Cre	Jackson Laboratory	Stock No: 008069
Mouse: SST-IRES-Cre	Jackson Laboratory	Stock No: 013044
Mouse: CaMKII-IRES-Cre	Jackson Laboratory	Stock No: 005359
Mouse: Ai 9	Jackson Laboratory	Stock No: 007909
Software and algorithms		
Origin 2021	Origin Lab	https://www.originlab.com/2021
Adobe Illustrator 24.0.1	Adobe	https://www.adobe.com/cn/products/illustrator.
IBM SPSS Statistics 21	IBM	http://www.spss.com.cn

(*Continued on next page*)

Continued

REAGENT or RESOURCE	SOURCE	IDENTIFIER
BORIS v. 7.9.6	Olivier Friard - Marco Gamba	http://www.boris.unito.it/
MATLAB 2018a	MathWorks	https://www.mathworks.com/products/matlab.

RESOURCE AVAILABILITY

Lead contact

Further information and requests for resources and reagents should be directed to and will be fulfilled by the lead contact, Dr. Wenting Wang (wwt0657@fmmu.edu.cn).

Materials availability

All requests for resources and reagents should be directed to and will be fulfilled by the lead contact, Dr. Wenting Wang (wwt0657@fmmu.edu.cn). This includes selective mouse lines, antibodies, viruses. All reagents will be made available on request after completion of a Material Transfer Agreement.

Data and code availability

- Data: Data reported in this paper will be shared by the lead contact upon request.
- Code: This paper does not report original codes.
- Additional information: Any additional information required to reanalyze the data reported in this paper is available from the lead contact upon request.

EXPERIMENTAL MODEL AND STUDY PARTICIPANT DETAILS

All experimental procedures were approved by the Institutional Animal Care and Use Committee of the Fourth Military Medical University (Approval No. IACUC-20220370)and conformed to the Guide for the Care and Use of Laboratory Animals published by the National Institutes of Health. All mice were maintained under a 12-h light/dark cycle at 22–25°C with *ad libitum* access to food and water under environmentally controlled conditions. C57BL/6J mice were purchased from the Experimental Animal Center of the Fourth Military Medical University. The PV-IRES-Cre, SST-IRES-Cre, CaMKII-IRES-Cre, and Ai 9 mice were obtained from the Jackson Laboratory (key resources table). All virus injections were administered to mice aged 2 months old, and all behavioral tests were carried out during the light phase. The experimenters were blinded to the genotype and experimental conditions. All the mice employed in the behavioral tests were male, and some females were used to provide morphological tests, the details were shown in the Table S1.

METHOD DETAILS

Virus and trace injection

Mice were anesthetized with isoflurane (4% for induction and 1.5% for maintenance), and their heads were fixed in a stereotaxic injection frame (RWD Life Science Inc., China). Injections into the brain were performed using a microinjection needle with a 10 μL microsyringe (Shanghai Gaoge Industry & Trade Co., LTD, China) to deliver the virus at a rate of 30 nL/min using a microsyringe pump (KD Scientific Inc., USA). The coordinates were defined as dorsal-ventral (DV) from the skull surface, anterior-posterior (AP) from bregma and medio-lateral (ML) from the midline (in mm). Following injection, the needle was held at the site for another 15 min to allow for diffusion.

The stereotaxic coordinates for the Ziv injection were as follows: anterior posterior (AP), -2.35 mm; medial lateral (ML), ±1.65 mm; and dorsal ventral (DV), -4.15 mm. The stereotaxic coordinates for the S1 injection were as follows: anterior posterior (AP), -1 mm; medial lateral (ML), ±3.05 mm; and dorsal ventral (DV), -1.5 mm. The stereotaxic coordinates for the CeA injection were as follows: anterior posterior (AP), -1.15 mm; medial lateral (ML), ±2.9 mm; and dorsal ventral (DV), -4.68 mm.

For retrograde monosynaptic tracing, helper viruses that contained rAAV-EF1α-DIO-EGFP-T2A-TVA and rAAV-EF1α-DIO-oRVG (1:2, 120nl) were co-injected into the Ziv (AP: -2.10 mm, ML: -0.77 mm, DV: -3.20 mm) of PV-IRES-Cre mice. After three weeks, the rabies virus RV-ENVA-ΔG-DsRed (120 nl) was injected into the same site of the Ziv.

Optogenetic manipulation

For ChR2 photostimulation, 470-nm light laser (5 ms, 20 Hz, with a 5-min light-on period that followed a 5-min light-off period, Newdoon Technology) was delivered via an optic cable (200-μm core, 0.37 NA, ThinkerTech, China). Laser power was 5-6 mW measured at the tip of the fiber, which was implanted 0.3 mm above the targeted nucleus. For eNPHR photostimulation, 593-nm light laser (5-min light-on period that followed a 5-min light-off period, Newdoon Technology) was delivered via an optic cable (200-μm core, 0.37 NA, ThinkerTech, China). Laser power was 6-9 mW measured at the tip of the fiber, which was implanted 0.3 mm above the targeted nucleus.

Grooming behavioral test

For all behavioural tests, animals were habituated for 2 h before testing. The behaviours of the animals were recorded in a test chamber (25 cm length, 25 cm width and 30 cm height) by a video camera (GUCEE, HD82-8MAF).

For spontaneous self-grooming model, the animal was acclimated to the test chamber for 3-5 min, and then the spontaneous activities were recorded for 30 min.

For oil-induced self-grooming model, the experimenter gently held the animal and dripped corn oil (100μL) onto its orofacial area and put the animal into the test chamber to acclimate for 3-5 min and start recording for 30 min.[12]

For stress-induced self-grooming model, firstly, the animal was tail-suspended for 20 minutes, then put into the test chamber to adapt for 3-5 min and then started to record for 30 min.

Behavioural analysis: The grooming was quantified manually by observer with the aid of a animal behavior video analysis software (Boris 8.0.9).[51] The observer was blind to the experimental conditions. For gross analysis of self-grooming, the number of grooming bouts, the duration of individual bout and therefore the total grooming time in the test period, were evaluated. Self-grooming was defined as when the animal licked, or used the forelimb to stroke, its own body parts including the paws, nose, eyes, head, body, legs, tail and genital. An interruption of 6 s or more separated two individual bouts.[50]

Fiber photometry

Fiber photometry was used to record calcium signals using a commercialized fiber photometry system (ThinkerTech, China) as described previously.[52] To record the fluorescence signals, a 488-nm laser beam (OBIS 488LS; Coherent) was reflected off a dichroic mirror (MD498, Thorlabs) that was focused by a ×10 objective lens (0.3 NA; Olympus) and coupled to an optical commutator (Doris Lenses). An optical fiber (230 μm OD, 0.37 NA) guided the light between the commutator and the implanted optical fiber. The laser power at the tip of the optical fiber was adjusted to 0.01–0.02 mW to decrease laser bleaching. Fluorescence was bandpass-filtered (MF525-39, Thorlabs), and an amplifier was used to convert the photomultiplier tube current output to a voltage signal. The analog voltage signals were digitalized at 500 Hz and recorded by a Power 1401 digitizer with Spike2 software (CED).

For data analysis, the fluorescence change was calculated as Z-score, the Z-score values of the animals in each group were averaged. To precisely analyze the changes in the fluorescence values across the scratching train, we defined the baseline period (-2 to 0 s relative to the behavior onse). To quantify the change in the level of calcium signal induced by self-grooming, the area under the curve (AUC) of Z-score in each time window defined was calculated.

Brain slice electrophysiology and optogenetics

Preparation of acute brain slices was performed according to the published work.[7,53] Briefly, the mice were anesthetized with isoflurane and transcardially perfused with ice-cold carbogenated (95% O_2, 5% CO_2) cutting solution containing the following: 115 mM choline chloride, 2.5 mM KCl, 1.25 mM NaH_2PO_4, 0.5 mM $CaCl_2$, 8 mM $MgCl_2$, 26 mM $NaHCO_3$, 10 mM D-(+)-glucose, 0.1 mM L-ascorbic acid and 0.4 mM sodium pyruvate (300–305 mOsm l^{-1}). Coronal slices (300 μm-thick) containing the Ziv were prepared using a vibratome (VT1200S, Leica). Whole-cell patch-clamp recordings were made using infrared differential interference contrast visualization at 28–30°C in artificial cerebral spinal fluid (ACSF) containing the following: 119 mM NaCl, 2.3 mM KCl, 1.0 mM NaH_2PO_4, 26 mM $NaHCO_3$, 11 mM D-(+)-glucose, 1.3 mM $MgSO_4$ and 2.5 mM $CaCl_2$ (pH 7.4, 295–300 mOsm l^{-1}). Patch pipettes were filled with a solution containing the following: 128 mM potassium gluconate, 10 mM HEPES, 10 mM phosphocreatine sodium salt, 5 mM lidocaine N-ethyl chloride, 1.1 mM EGTA, 5 mM ATP magnesium salt and 0.4 mM GTP sodium salt (pH 7.3, 300–305 mOsm l^{-1}). The recordings were obtained using a multiclamp 700B amplifier (Molecular Devices) filtered at 5 kHz and sampled at 20 kHz with a Digidata 1550B. Clampex 10.7 was used for acquisition and analysis. For EPSCs recordings, the cell membrane potential was held at -70 mV in the presence of 1 μM TTX, 50 μM 4-AP, and 50 μM NBQX. For IPSCs recordings, the cell membrane potential was held at -70 mV in the presence of 1 μM TTX, 50 μM 4-AP, and 10 μM bicuculline.

Immunohistochemistry

Mice were anesthetized with isoflurane and sequentially perfused with saline and PBS containing 4% PFA. Post-fixation of the brain was avoided to optimize immunohistochemistry. Brains were incubated in PBS containing 30% sucrose until they sank to the bottom. Cryostat sections (35 mm) were collected, incubated 2h with blocking solution (PBS containing 10% donkey serum), and then incubated with primary antibodies (key resources table) overnight. Primary antibodies were washed three times with PBS before incubation with secondary antibodies (key resources table) for 3 h at room temperature. The sections were rinsed in PBS and counterstained with DAPI and mounted. Sections were imaged with an Olympus FV3000 confocal microscope or Olympus VS 200 epifluorescence microscope. Confocal images were analyzed with Imaris7.9 software.

QUANTIFICATION AND STATISTICAL ANALYSIS

Statistical analyses were performed using Origin 2021 and MATLAB 2018b (MathWorks). Statistical significance was set at $P < 0.05$, and all statistical parameters are reported in the figure legends. The normality test was performed using the Kolmogorov-Smirnov or Shapiro-Wilk test. For the analysis of immunostaining data, one-way ANOVA with a post hoc least significant difference (LSD) test or

an unpaired t-test was used. For the analysis of the behavioral data of the lesion and optogenetic experiments, a paired t-test or a Wilcoxon signed-rank test was used. For the analysis of the behavioral data, an unpaired t-test was used. For normally distributed fiber photometry data, a repeated measures ANOVA was firstly performed. If significant main effects were found, a simple effect analysis was performed. When significant main effects were not found, unpaired and paired t-test were used to compare the effects of the variables. For non-normal fiber photometry data, the Friedman test was used, followed by the Wilcoxon signed-rank test and Mann-Whitney U test to compare the effects of the variables.